

Brief Report

Assessment of the Catastrophic Asia Floods and Potentially Affected Population in Summer 2020 Using VIIRS Flood Products

Sanmei Li ¹, Mitchell D. Goldberg ², William Sjoberg ², Lihang Zhou ² , Sreela Nandi ², Nazmi Chowdhury ², William Straka III ³, Tianshu Yang ¹  and Donglian Sun ^{1,*}

¹ Department of Geography and Geoinformation Science, George Mason University, Fairfax, VA 22030, USA; slia@gmu.edu (S.L.); tyang4@masonlive.gmu.edu (T.Y.)

² NOAA JPSS Program Office, Lanham, MD 20706, USA; mitch.goldberg@noaa.gov (M.D.G.); bill.sjoberg@noaa.gov (W.S.); Lihang.Zhou@noaa.gov (L.Z.); Sreela.Nandi@noaa.gov (S.N.); nazmi.chowdhury@noaa.gov (N.C.)

³ Space Science and Engineering Center (SSEC), University of Wisconsin, Madison, WI 53706 20740, USA; william.straka@ssec.wisc.edu

* Correspondence: dsun@gmu.edu; Tel.: +1-703-993-4736

Received: 25 August 2020; Accepted: 24 September 2020; Published: 28 September 2020



Abstract: Since 2 June 2020, unusual heavy and continuous rainfall from the Asian summer monsoon rainy season caused widespread catastrophic floods in many Asian countries, including primarily the two most populated countries, China and India. To detect and monitor the floods and estimate the potentially affected population, data from sensors aboard the operational polar-orbiting satellites Suomi National Polar-Orbiting Partnership (S-NPP) and National Oceanic and Atmospheric Administration (NOAA)-20 were used. The Visible Infrared Imaging Radiometer Suite (VIIRS) with a spatial resolution of 375 m available twice per day aboard these two satellites can observe floodwaters over large spatial regions. The flood maps derived from the VIIRS imagery provide a big picture over the entire flooding regions, and demonstrate that, in July, in China, floods mainly occurred across the Yangtze River, Hui River and their tributaries. The VIIRS 5-day composite flood maps, along with a population density dataset, were combined to estimate the population potentially exposed (PPE) to flooding. We report here on the procedure to combine such data using the Zonal Statistic Function from the ArcGIS Spatial Analyst toolbox. Based on the flood extend for July 2020 along with the population density dataset, the Jiangxi and Anhui provinces were the most affected regions with more than 10 million people in Jingdezhen and Shangrao in Jiangxi province, and Fuyang and Luan in Anhui province, and it is estimated that about 55 million people in China might have been affected by the floodwaters. In addition to China, several other countries, including India, Bangladesh, and Myanmar, were also severely impacted. In India, the worst inundated states include Uttar Pradesh, Bihar, Assam, and West Bengal, and it is estimated that about 40 million people might have been affected by severe floods, mainly in the northern states of Bihar, Assam, and West Bengal. The most affected country was Bangladesh, where one third of the country was underwater, and the estimated population potentially exposed to floods is about 30 million in Bangladesh.

Keywords: Asia floods; summer 2020; VIIRS; flood mapping; population potentially exposed (PPE) to floods

1. Introduction

Floods are the most devastating, frequent, and widespread natural disaster, affecting about, on average, 80 million people per year around the world, and causing more death and property damage

than any other natural phenomena [1,2]. Every year, flood disasters cause huge economic losses and life disruption all over the world [2]. This year, the low-pressure systems of Asia's summer monsoon have been unusually strong and stationary [3], allowing them to transfer even more water vapor from the Indian and Pacific oceans to South and East Asia. Since 2 June 2020, the unusually heavy and continuous rainfall during the Asian summer monsoon rainy season resulted in widespread severe floods in many Asian countries, including the two most populated countries, China and India.

In China, major floods mainly occurred across the Yangtze River, Huai River, and their tributaries [4]. In June, the impacted regions include the upper and middle basin of the Yangtze River and its tributaries in several provinces, including Sichuan, Hubei, as well as Hunan with 14 million people affected [5]. In July, heavy rainfall attacked central and eastern China [6], and flooding became widespread and deadly. Flooding waters propagated to lower regions of the Yangtze basin and Huai River basin, such as Jiangxi, Anhui, Jiangsu, and Zhejiang. The worst flooding occurred in Jiangxi Province and Anhui Province. The catastrophic floods in Jiangxi affected roughly 5.21 million people, primarily around the Poyang Lake and its tributaries. This catastrophic Asian summer flooding caused severe property damage and a high death toll. According to the South China Morning Post, by the end of July, 54.8 million people in 27 provinces had been affected, and at least 219 people were reported as dead or missing, and 54,000 houses were destroyed [7]. Maybe one of the most affected countries was Bangladesh, where one third of the country was underwater. More than 5.4 million people were affected and at least 100 died as of July 28 [8]. In India, the major affected regions were limited to the northern states of Bihar, Assam, and West Bengal. The worst impacted States were Assam and Bihar. Till August, more than 17 million people experienced flooding, and the number of fatalities reached 1082 [9]. The economic loss is estimated at 178.9 billion yuan or USD 25.7 billion in China alone, once again highlighting the importance of flood monitoring in protecting lives and properties.

Developing countries usually suffer higher casualties from natural hazards than developed countries. In developing countries, thousands of victims are killed or injured by natural disasters every year [10]. Mitigating the losses of human lives and properties from natural disasters in developing countries is critical to reduce the poverty [11]. Better assessment of natural hazard impacts on human in developing countries will need advanced study combining conventional data on population with satellite observations.

Satellite-based flood maps have been proven to be very helpful for analysis and evaluation of the spatial extent of flooding events and can provide valuable guidance for rescue and relief efforts [12]. Operational and environmental satellites with large spatial coverage and high temporal resolution show advantages for mapping, monitoring, and analyzing large-scale floods such as the catastrophic Asia floods in this summer. The NOAA (National Oceanic and Atmospheric Administration) operational polar orbiting satellites can provide observations twice per day for mid-latitude regions, over large spatial regions with no data cost and no risk to get access to the dangerous flooding areas, and demonstrate advantages for large-scale flood mapping and monitoring [13–17]. The Advanced Very-High-Resolution Radiometer (AVHRR) on board the previous Polar Operational Environmental Satellites (POES) series had been widely used for flood detection and mapping [13–17]. The Moderate-Resolution Imaging Spectroradiometer (MODIS) onboard the NASA (National Aeronautics and Space Administration) scientific instrument EOS (Earth Observing System) provides similar but enhanced capability to AVHRR, because MODIS can provide flood mapping at a 250 m spatial resolution, better than the AVHRR 1 km resolution. The MODIS have been successfully applied for flood detection and monitoring with a 250 m spatial resolution [18–26]. Most recently, the VIIRS (Visible Infrared Imaging Radiometer Suite) [27], onboard the Suomi National Polar-orbiting Partnership (S-NPP) satellite, and the Joint Polar Satellite System (JPSS) and now as the new NOAA series, succeeds the MODIS for flood mapping. The VIIRS imagery with a 375 m spatial resolution in the short-wave IR bands and wide 3000 km swath width have demonstrated advantages for flood detection [28–30]. Since the imagers onboard the operational and environmental satellites are usually optical sensors, which can be contaminated by clouds. Microwave remote

sensing instruments, including passive microwave (MW) instruments [31–34] and active airborne synthetic aperture radar (SAR) imagery [35], can penetrate clouds and provide flood detection under cloudy conditions. However, passive MW sensors usually have very coarse spatial resolutions (10–25 km) [31–34]. Even though high-resolution SAR data (10–30 m) can provide very valuable surface information under almost all sky conditions, it usually has limited spatial coverage and a long revisit time (6–12 days) [35]. Recently, geostationary satellites, GOES-R series with a 5 min temporal resolution, allowing us to capture some clear sky observations, have been utilized to help mitigate the cloud contamination problem [36,37]. Multi-day composite VIIRS flood maps have been used to filter the cloud contamination and obtain the maximum flood extent; they are very useful for flood damage assessment after the flooding events [36].

Using a geographic information system (GIS) system, the population cells can be clipped to satellite-derived flood footprints to estimate the ‘population potentially exposed’ (PPE) to flood events [38]. The objective of this study is to map and analyze the catastrophic Asia floods and estimate the affected population in summer 2020 using VIIRS imagery onboard both the S-NPP (Suomi National Polar-Orbiting Partnership) and NOAA-20 polar-orbiting weather satellites. The VIIRS-derived flood footprints will be combined with population databases and ArcGIS (version 10.4.1) for human impact assessment in the catastrophic Asia flood events during summer 2020.

2. Data and Methods

2.1. Data Used

The VIIRS data are acquired from the NOAA operational feed, which provides data globally to users for each orbit (S-NPP) or half-orbit (NOAA-20). The datasets used for VIIRS flood mapping are listed below:

- VIIRS SDR (Sensor Data Record) data at Imager bands 1, 2, 3 and 5 with 375-m spatial resolution.
- Geolocation data, including longitude, latitude, solar zenith angles, solar azimuth angles, sensor zenith angles and sensor azimuth angles.
- VIIRS Intermediate Cloud Mask Product with 750-m resolution.
- Static ancillary datasets include:
 - The IGBP (International Geosphere-Biosphere Programme) global land cover;
 - Global land/sea mask;
 - MODIS 250-m global water mask (MOD44W) [18];
 - Water layer in the National Land Cover Database 2006 [39].
- The population count dataset for China, Bangladesh, and India in 2020 at a resolution of 3 arc-seconds (approximately 100 m at the equator) is obtained from the WorldPop [40]. This database has been continuously updated every year.

2.2. Methods

2.2.1. VIIRS Flood Detection

The physical basis for flood detection with the VIIRS imagery is the spectral characteristics in the VIIRS visible (VIS), near infrared (NIR), and short-wave infrared (SWIR) channels. The main algorithms include a decision-tree method by integrating the reflectance in the VIIRS imager channels and a set of spectral indices to classify water surface from vegetation, bare land, and snow/ice surface [19–21,30], a geometry-based cloud-shadow algorithm to separate cloud shadows from VIIRS flood maps [28], an object-based terrain-shadow algorithm to discriminate terrain shadows from VIIRS flood maps [29], and a dynamic nearest neighboring searching (DNNS) method to calculate water fractions [21]. The derived water fractions are then compared with a water reference map at normal conditions to identify flooding water. In the VIIRS flood maps, the floodwater fraction is marked

as water percentage in a pixel from 1% to 100%. A comprehensive introduction to the VIIRS flood algorithm can be found from a referenced paper [30]. VIIRS flood algorithms and products have been extensively validated and evaluated [30].

2.2.2. Multiple-Day Composition

Because VIIRS is an optical sensor, the images may be contaminated by clouds. To filter out cloud cover, a multi-day composition process is applied to derive the maximal flood extent. With the near-real-time (NRT) VIIRS flood maps during a period, a pixel is assigned as a flooding pixel in the composited flood map as long as it is detected as a flooding pixel in any flood map during that period, and the maximum flood water fraction among all the NRT flood maps is used as its composited water fraction. If a pixel is not detected as flood but is detected as dryland in any NRT flood maps, then it is assigned as a dryland pixel in the composited flood map. The composition process is illustrated in Figure 1. In this way, the composited flood map shows the maximal clear-sky coverage with the maximal floodwater fractions during an appointed period.

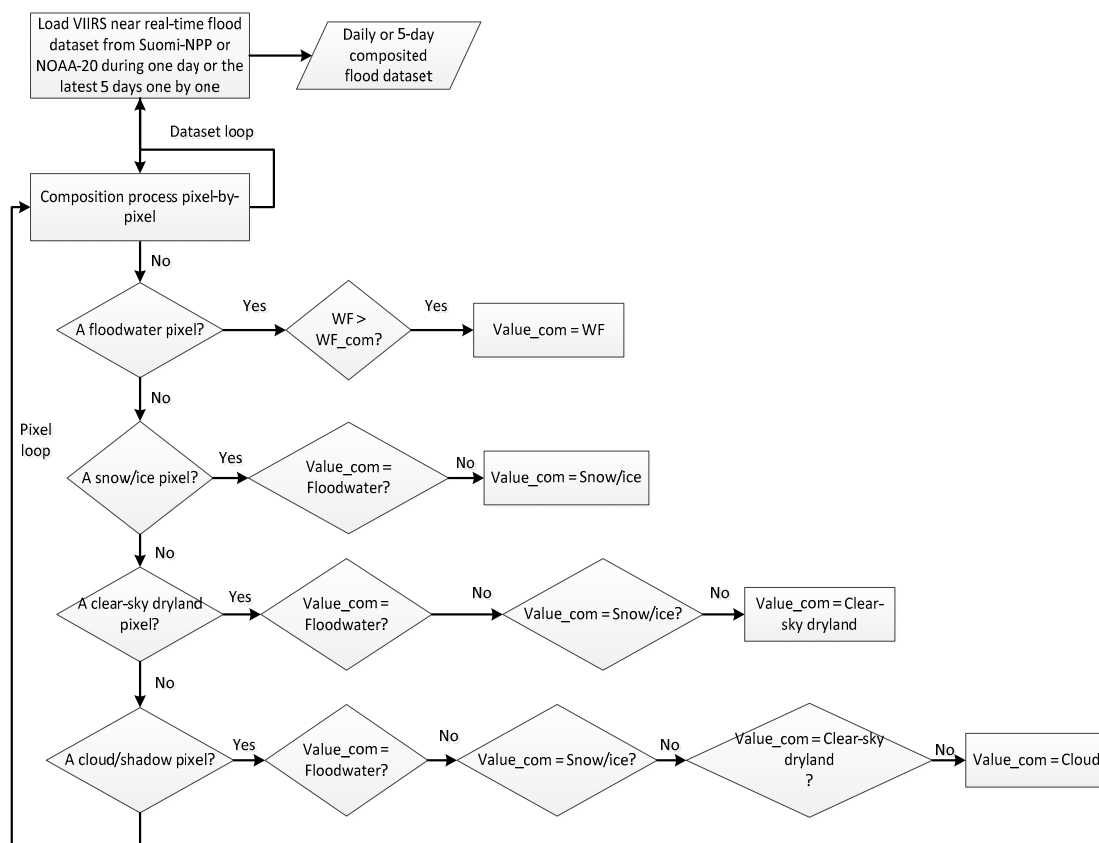


Figure 1. Flow chart of the composition process.

2.2.3. Spatial Analysis

The Geographic Information System (GIS) has been widely used to integrate different spatial data for visualization and further spatial analysis to estimate probable damage due to floods [41,42]. Using GIS software, the population grids can be clipped to flood footprints to estimate the 'population potentially exposed' (PPE) to flood events [38,43]. With the ArcGIS Zonal Statistics tool, a statistic is calculated for each zone defined by a zone dataset (a flooded district here), based on values from another dataset (a value raster, like population data here). A single output value is computed for every zone (flooded district, like a city or county) in the input zone dataset (VIIRS flood maps here). The sum of all the cell values in each zone is assigned to all cells in that zone. The VIIRS-derived

flood footprints are loaded into the ArcGIS system. Both VIIRS flood and population datasets are projected in the WGS1984 coordinate system. Based on the VIIRS detected floodwater, the Zonal Statistic Function in the ArcGIS Spatial Analyst toolbox is further used to estimate the total population potentially exposed to the flood events for each country. Figure 2 shows the study areas.

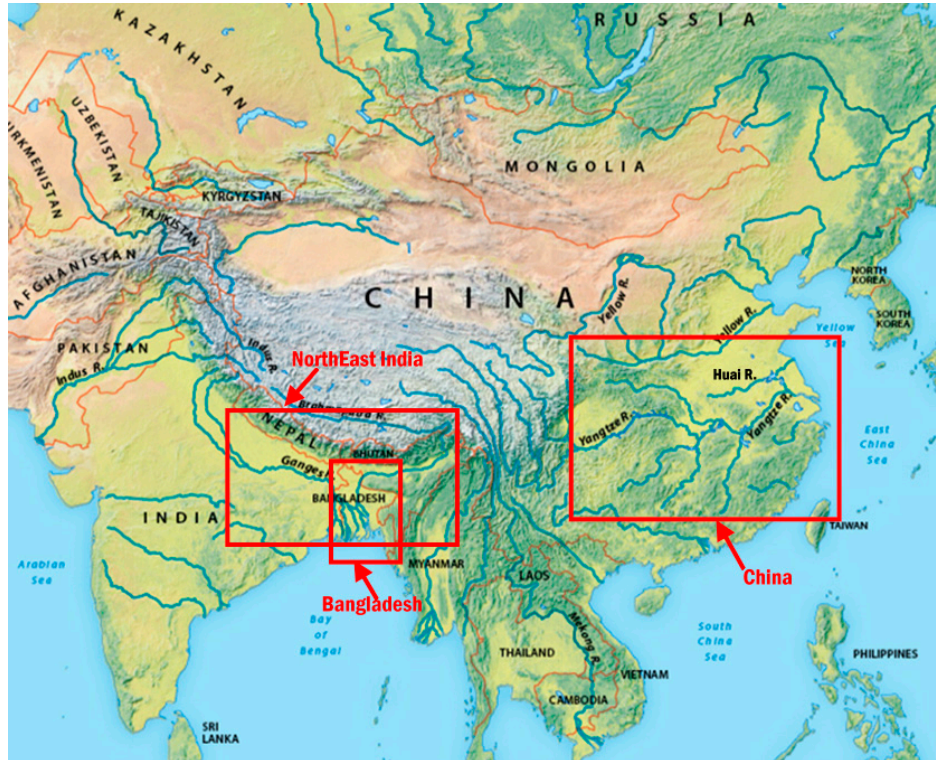


Figure 2. Study areas.

3. Results

The VIIRS 5-day composite flood maps from 28 July to 1 August 2020 are shown in Figure 3. By the end of July, flooding across the Huai River and its tributaries became severe. The Yangtze River and the Huai River were inundated at the same time and soon evolved into major floods. The affected regions include not only the upper and middle river basin of the Yangtze and its tributaries such as Sichuan, Hubei, and Hunan, but also extended to the lower regions of the Yangtze basin and Hua River basin such as Jiangxi, Anhui, Jiangsu, and Zhejiang. As shown in Figure 3 (upper), one of the worst flooded regions is located in Jiangxi Province along the Poyang Lake. Figure 3 demonstrates the advantages of an operational weather satellite with large spatial coverage. Such satellites enable watching a flood over the entirety of China. The VIIRS flood map can show the flood extents over both Yangtze River and Huai River and their tributaries.

The remotely sensed flood maps obtained from VIIRS were implemented into the ArcGIS to estimate the population potentially exposed to flooding. Utilizing the 2020 WorldPop [40] population distribution map, and overlaying it on the areas of likely inundated regions (Figure 3 upper) through the zonal statistics in the ArcGIS shows an example of how VIIRS flood maps can potentially help decision makers to locate the potentially exposed population within the inundated areas during this catastrophic flood period. According to the spatial analysis with the ArcGIS (Figure 3 lower), the total affected population is about 37,371,605 in Anhui province, 807,771 in Henan province, 2,722,861 in Hubei province, 3,148,590 in Hunan province, 9,964,559 in Jiangxi province, 181,672 in Shanghai, and 1,736,842 in Zhejiang province. The most deadly rejoinings include Fuyang and Luan in Anhui province along the Huai River basin, and Jingdezhen and Shangrao in Jiangxi province along the Yangtze River floodplains, where more than 10 million people might have been affected by the

floodwaters. The total estimated PPE is about 55.3 million in China, which is very close to the reported 54.8 million victims [7].

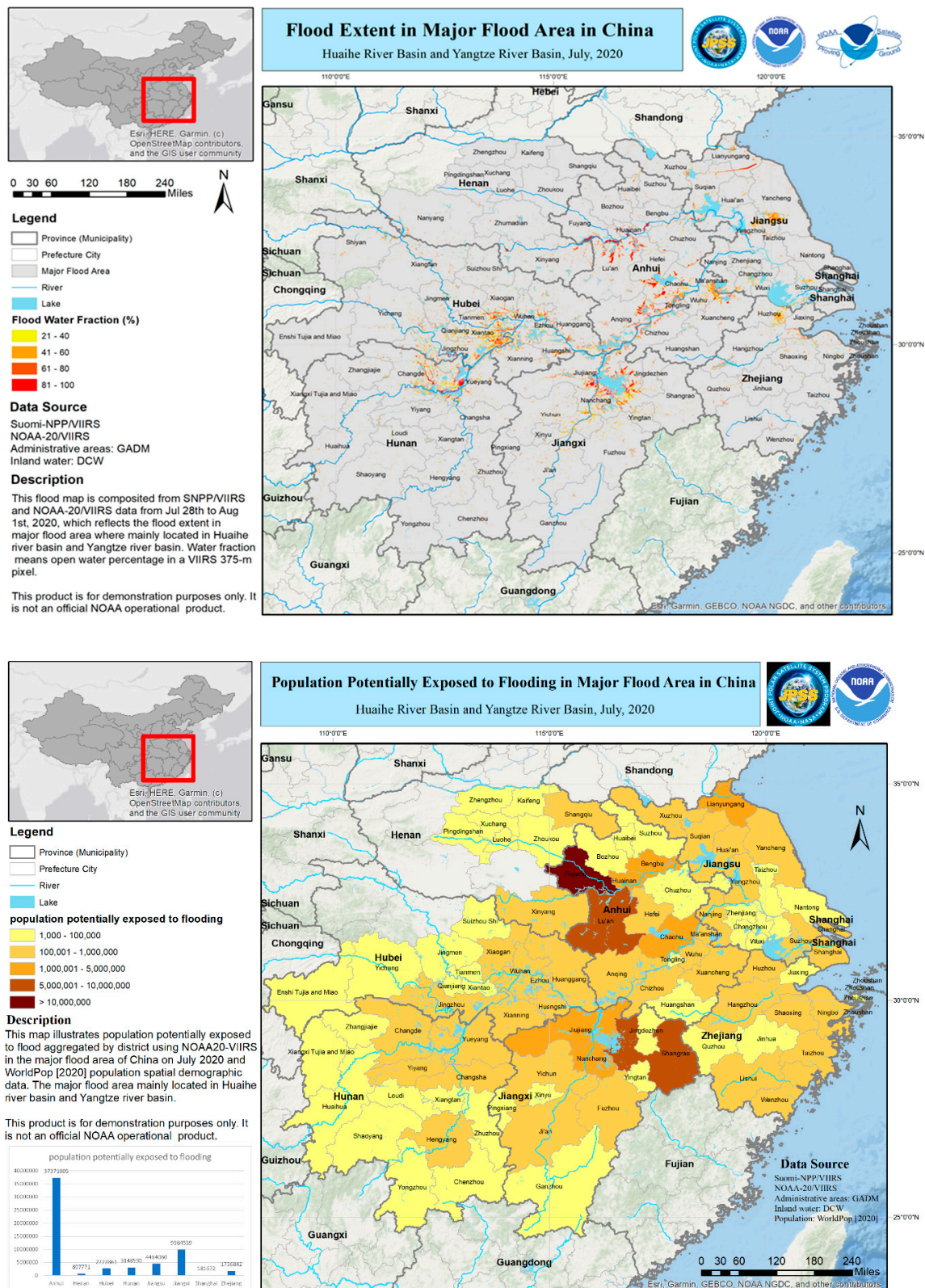


Figure 3. VIIRS 5-day composite flood map from 28 July to 1 August (upper) and the estimated population potentially exposed to flooding (lower) in July 2020 in China.

As mentioned previously, the unusually heavy rainfall from the 2020 summer monsoon also resulted in widespread severe flooding in South Asia, including India, Bangladesh, and Myanmar (Burma). Figure 4 shows the flood situation across Bangladesh, Myanmar (Burma), and India. As shown in Figure 4, two main Himalayan rivers—the Brahmaputra and the Ganges—that flow across Bangladesh and India, and the regions around the Brahmaputra River, were severely inundated. One third of Bangladesh, including Jamalpur, Tangail, Sylhet, and Barddhaman, was underwater. In Myanmar, major floods occurred at the west and south coastal regions, and along the Ayeyarwady River.

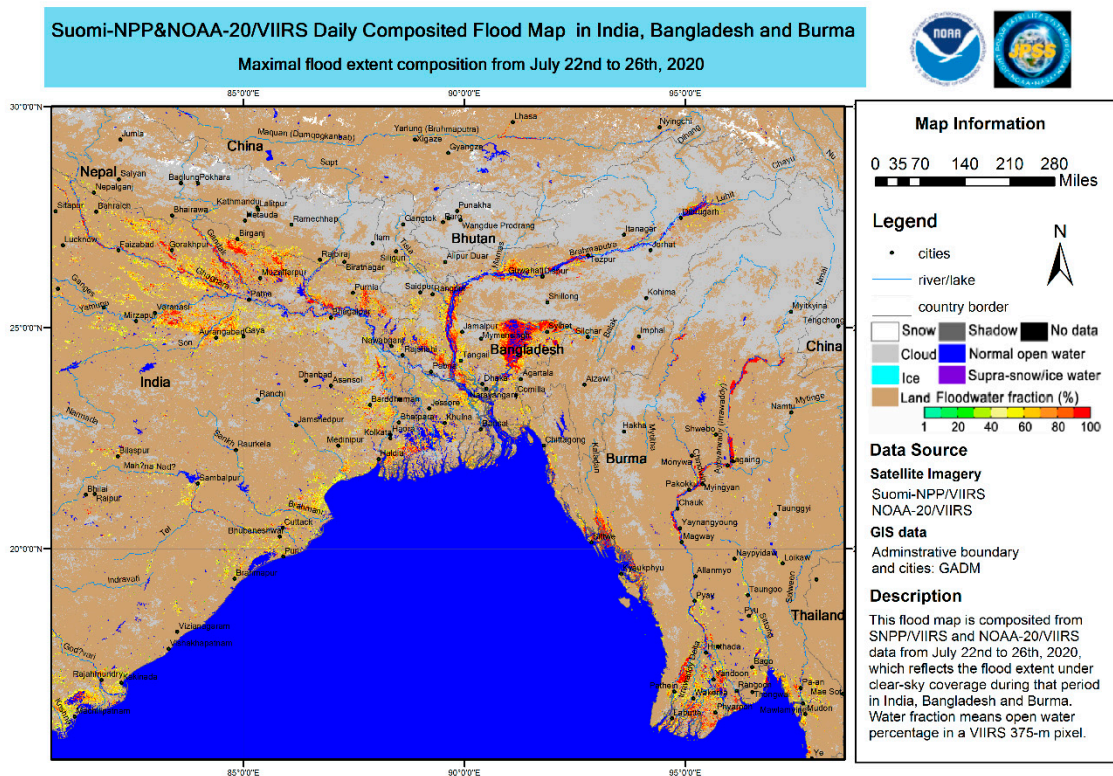


Figure 4. Visible Infrared Imaging Radiometer Suite (VIIRS) 5-day composite flood maps from 22 to 26 July 2020, across Bangladesh, Burma, and India.

Figure 5 illustrates the potentially exposed population to floods (cumulative) aggregated by district using the NOAA20-VIIRS-derived flood map in Bangladesh between the 22nd and the 26th of July, 2020, and Worldpop spatial demographic data [40]. According to the estimate from the spatial analysis with the ArcGIS, the worst affected districts are mainly located in Dhaka, Sylhet, and Rajshahi divisions, with a PPE of over 1.3 million. According to the estimate, the total population potentially exposed to floods is about 9,889,899 in Dhaka, 5,118,810 in Chittagong, 4,926,018 in Sylhet, 4,409,792 in Rajshahi, 3,181,396 in Rangpur, 2,144,122 in Khulna, and 725,797 in Barisal. About 30 million people in Bangladesh were exposed or living close to flooded areas. The estimated 30 million PPE is much higher than the reported 5.4 million flood victims in Bangladesh [8]. The Bangladesh 2020 population is estimated at 164,689,383 people; if one third of Bangladesh was reported to be underwater in July 2020, the estimated 30 million population potentially exposed to floods should make sense.

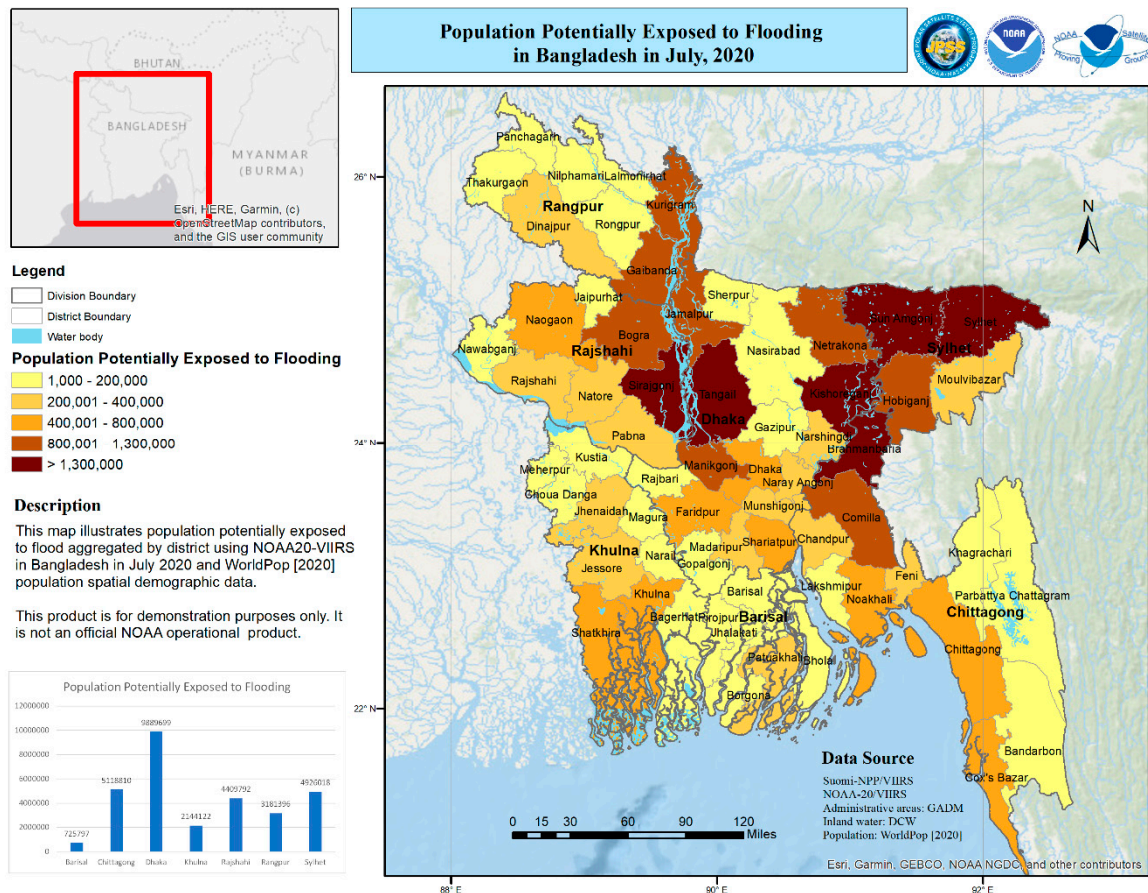


Figure 5. Estimated population potentially exposed to flooding in July 2020 in Bangladesh.

The VIIRS composited flood map from 29 July to 2 August (Figure 6 upper) show details about floods in north/northeast India during this time period. The worst inundated states within India were Uttar Pradesh, Bihar, Assam, and West Bengal. As shown in Figure 6 (lower), the majority of the population exposed to flood was limited to northern states of Bihar, Assam, and West Bengal. The worst impacted States are Bihar and Assam. It is estimated that the total population potentially exposed to floods is 32,360,188 in the poorest Bihar state, 9,491,897 in Assam state, 4,434,680 in Uttar Pradesh, and 12,533,403 in West Bengal (Figure 6 lower). The estimated total PPE is about 40 million in India. Compared to the report [9], more than 7.4 million people in Bihar, and over 3.5 million people in Assam, and more than 17 million people in entire India were affected by floods.

4. Discussion

Operational weather satellites such as the S-NPP/JPSS satellites, which are the first two satellites in a series of NOAA polar orbiting satellites, have the strengths of large spatial coverage and frequent observations. The JPSS series will provide critical observations for the environment and the Earth system until the late 2030s. The VIIRS flood maps can provide big pictures of flood over large spatial regions and can be used for damage assessment. Moreover, the VIIRS flood maps can be frequently available and used as guidance for decision makers for rescue efforts. The VIIRS global flood products, including VIIRS near-real-time flood product, VIIRS daily composited flood product, and VIIRS 5-day composited flood product, are now routinely generated in Space Science and Engineering Center (SSEC) of the University of Wisconsin-Madison, where direct broadcast VIIRS data can be obtained. All these products are now available from the SSEC’s Real Earth front page [44]. The VIIRS near-real-time, daily and 5-day composited flood maps since October 2019, including all the flood maps shown here,

can be obtained from the NOAA JPSS Proving Ground Global Flood Products archived at George Mason University [45].

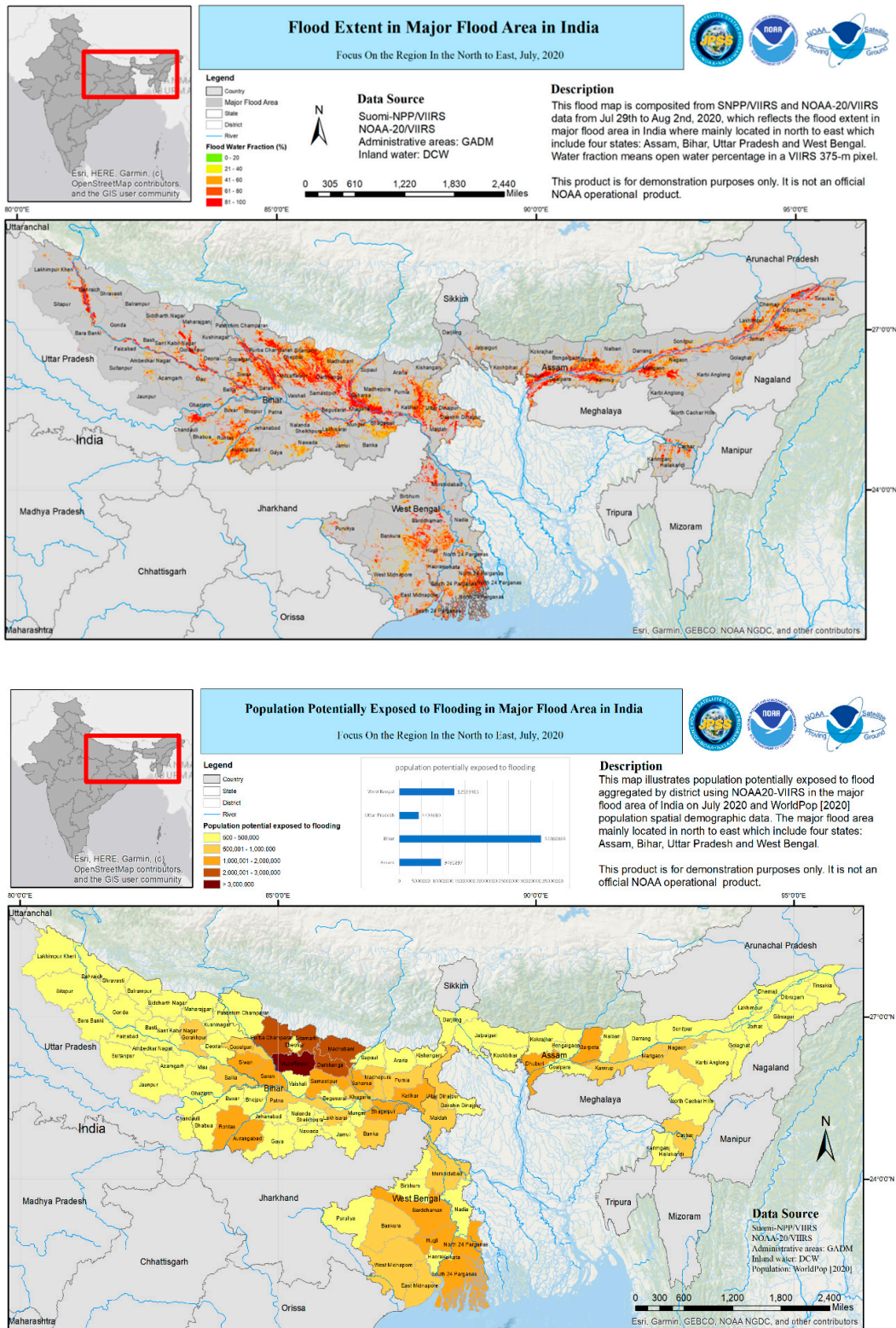


Figure 6. VIIRS 5-day composite flood maps from 29 July to 2 August (upper) and the estimated population potentially exposed to flooding (lower) in July 2020 in India.

It is expected that operational weather satellites such as the new NOAA series with daily observations, in combination with other upcoming LEO (low Earth orbit) and GEO (geosynchronous) sensors, will continue playing a significant role in mapping and monitoring floods over large spatial areas, especially like this large-scale Asia flood event.

In this study, VIIRS flood products are applied for assessing the potential population affected by the floods, which is directly relevant to disaster response and rescue efforts. The resolution of the VIIRS flood footprint is different from the population resolution and may generate errors in the PPE estimation. There are also some technical limitations to include flash flood impacts on human, because 5-day composite flood maps are used to estimate the PPE, and the flooding water from flash floods usually cannot be captured by the satellites.

While the estimated PPE in China is very close to the reports, the estimated total PPE in Bangladesh and India are much higher than the reported numbers. This may be because the population data used for PPE estimation is static, while, in reality, some people might have been evacuated before the flooding. Another reason is that all VIIRS-based flood footprints, including minor floods with a flooding water fraction less than 20%, are used to estimate the population within the inundated areas, while, in a real situation, small floods may not affect people.

5. Conclusions

In this study, the flood maps derived from VIIRS observations were implemented into the ArcGIS system and combined with the world population dataset to estimate the potentially affected population by floods during this summer catastrophic flooding events across South and East Asia. According to the spatial analysis with the ArcGIS, Jiangxi provinces and Anhui province in China were most deadly impacted by the severe flooding. There were approximately over 10 million people in each city or region at Jingdezhen and Shangrao in Jiangxi province along the Yangtze River floodplains, and Fuyang and Luan in Anhui province around the Huai River basin, and approximately about 55 million people in China might have been affected by the floodwaters. The unusually heavy summer monsoon rainfall also caused widespread severe flooding in Bangladesh, Myanmar, and India. Two main Himalayan rivers—the Brahmaputra and the Ganges—that flow across Bangladesh and India, and the nearby regions, were severely inundated. One third of Bangladesh was underwater. The north/northeast of India also experienced severe floods, and the worst inundated states include Uttar Pradesh, Bihar, Assam, and West Bengal. It is estimated that about 40 million people in the northern states Bihar and Assam might be potentially influenced by the severe floods. The estimated total PPE is 55 million in China, and very close to the reported 54.8 million affected population [7]. The estimated 40 million PPE in India is much higher than the report claiming at least 17 million affected people [9], while, in Bangladesh, the estimated PPE is about 30 million, also higher than the reported 5.4 million affected people. Considering the Bangladesh 2020 population estimated at 164,689,383 people, if one third of Bangladesh was reported to be underwater in July 2020, the estimated 30 million PPE should be reasonable.

Author Contributions: Methodology, S.L., T.Y., and D.S.; software, S.L., and T.Y.; validation, S.L. and D.S.; formal analysis, S.L., T.Y., and D.S.; investigation, S.L., T.Y., W.S.III, and D.S.; data curation, S.L., and T.Y.; writing—original draft preparation, D.S., and S.L.; writing—review and editing, D.S., S.L., W.S.III, T.Y., M.D.G., W.S. and L.Z.; visualization, T.Y., S.L., and D.S.; supervision, M.D.G., W.S., L.Z., S.N., N.C.; project administration, M.D.G., W.S., S.N., N.C., and L.Z.; funding acquisition, M.D.G., L.Z., S.N., and N.C. All authors have read and agreed to the published version of the manuscript.

Funding: This research was funded by NOAA JPSS Program Office through the NSF I/UCRC for Spatiotemporal Innovation Center.

Acknowledgments: The VIIRS flood product is routinely running at the Space Science and Engineering Center (SSEC) and Geographic Information Network of Alaska (GINA). The contents are solely the opinions of the authors and do not constitute a statement of policy, decision, or position on behalf of NOAA or the U. S. Government. We thank the reviewers and editors for their constructive and helpful comments!

Conflicts of Interest: The authors declare no conflict of interest.

References

1. Kundzewicz, Z.W.; Schellnhuber, H.J. Floods in the IPCC TAR perspective. *Nat. Hazards* **2004**, *31*, 111–128. [[CrossRef](#)]
2. International Federation of the Red Cross and Red Crescent Societies (IFRC). *World Disasters Report*; Oxford University Press: Oxford, UK, 2008; ISBN 978-92-9139-156-1.
3. Clift, P.D.; Holbourn, A.; France-Lanord, C.; Zheng, H. *Evolution of the Asian Monsoon*; Eos: Washington, DC, USA, 2020; p. 101. [[CrossRef](#)]
4. Yu, Z. Floods in China: Can the Three Gorges Dam weather once-in-a-century massive floods in the Yangtze River? *Think China*, 11 July 2020.
5. Lew, L. After coronavirus, Flooding Hits Southern China with 14 Million Affected. *South China Morning Post*, 29 June 2020.
6. More Chinese Regions Brace for Floods as Storms Shift East. *Reuters*, 29 June 2020.
7. Yan, L. Emergency Management Division: Floods caused 5481.1 affected people in 27 provinces in China. *China News*, 28 July 2020. (In Chinese)
8. ReliefWeb. Bangladesh: Floods and Landslides—July 2020. Available online: <https://reliefweb.int/disaster/fl-2020-000161-bgd> (accessed on 15 August 2020).
9. ReliefWeb. India: Floods and Landslides—July 2020. Available online: <https://reliefweb.int/disaster/fl-2020-000164-ind> (accessed on 15 August 2020).
10. Rodriguez, J.; Vos, F.; Below, R.; Guha-Sapir, D. *Annual Disaster Statistical Review 2008: The Numbers and Trends*; CRED: Brussels, Belgium, 2008.
11. Christophos, I.; Mitchell, J.; Liljelund, A. Re-framing risk: The changing context of disaster mitigation and preparedness. *Disasters* **2001**, *25*, 185–198. [[CrossRef](#)] [[PubMed](#)]
12. Schumann, G.J.; Domeneghetti, A. Exploiting the proliferation of current and future satellite observations of rivers. *Hydrol. Process.* **2016**, *30*, 2891–2896. [[CrossRef](#)]
13. Barton, I.J.; Bathols, J.M. Monitoring floods with AVHRR. *Remote Sens. Environ.* **1989**, *30*, 89–94. [[CrossRef](#)]
14. Ali, A. Study of river flood hydrology in Bangladesh with AVHRR data. *Int. J. Remote Sens.* **1989**, *10*, 1873–1892. [[CrossRef](#)]
15. Sheng, Y.; Xiao, Q. Water Identification in Cloud-contaminated NOAA/AVHRR Imagery. *Remote Sens. Environ. China* **1994**, *9*, 247–255.
16. Sheng, Y.; Su, Y.; Xiao, Q. Challenging the cloud-contamination problem in flood monitoring with NOAA/AVHRR imagery. *Photogramm. Eng. Remote Sens.* **1998**, *64*, 191–198.
17. Sheng, Y.; Gong, P. Quantitative dynamic flood monitoring with NOAA AVHRR. *Int. J. Remote Sens.* **2001**, *22*, 1709–1724. [[CrossRef](#)]
18. Carroll, M.; Townshend, J.; DiMiceli, C.; Noojipady, P.; Sohlberg, R. A New Global Raster Water Mask at 250 Meter Resolution. *Int. J. Digit. Earth* **2009**, *2*, 291–308. [[CrossRef](#)]
19. Sun, D.L.; Yu, Y.; Goldberg, M.D. Deriving water fraction and flood maps from MODIS images using a decision tree approach. *IEEE J. Sel. Top. Appl. Earth Obs. Remote Sens.* **2011**, *4*, 814–825. [[CrossRef](#)]
20. Sun, D.L.; Yu, Y.; Zhang, R.; Li, S.; Goldberg, M.D. Towards Operational Automatic Flood Detection Using EOS/MODIS data. *Photogramm. Eng. Remote Sens.* **2012**, *78*, 637–646. [[CrossRef](#)]
21. Li, S.; Sun, D.; Yu, Y.; Csiszar, I.; Stefanidis, A.; Goldberg, M.D. A New Shortwave Infrared (SWIR) Method for Quantitative Water Fraction Derivation and Evaluation with EOS/MODIS and Landsat/TM data. *IEEE Trans. Geosci. Remote Sens.* **2012**, *51*, 1852–1862. [[CrossRef](#)]
22. Li, S.; Sun, D.; Goldberg, M.D.; Stefanidis, A. Derivation of 30-m-resolution Water Maps from TERRA/MODIS and SRTM. *Remote Sens. Environ.* **2013**, *134*, 417–430. [[CrossRef](#)]
23. Schumann, G.; Wells, G.; Adler, R.; Brakenridge, R.; Bolten, J.; Murray, J.; Slayback, D.; Policelli, F.; Kirschbaum, D.; Wu, H.; et al. Unlocking the full potential of Earth observation during the 2015 Texas flood disaster. *Water Resour. Res.* **2016**, *52*, 3288–3293. [[CrossRef](#)]
24. Schumann, G.J.-P. Flood response using Earth observation data and products. *EOS* **2016**, *97*. [[CrossRef](#)]
25. Schumann, G.J.-P. Preface: Remote sensing in flood monitoring and management. *Remote Sens.* **2015**, *7*, 17013–17015. [[CrossRef](#)]
26. Martinis, S.; Twele, A.; Strobl, C.; Kersten, J.; Stein, E. A multi-scale flood monitoring system based on fully automatic MODIS and TerraSAR-X processing chains. *Remote Sens.* **2013**, *5*, 5598–5619. [[CrossRef](#)]

27. Cao, C.; De Luccia, F.J.; Xiong, X.; Wolfe, R.; Weng, F. Early On-Orbit Performance of the Visible Infrared Imaging Radiometer Suite Onboard the Suomi National Polar-Orbiting Partnership (S-NPP) Satellite. *IEEE Trans. Geosci. Remote Sens.* **2014**, *52*, 1142–1156. [[CrossRef](#)]
28. Li, S.; Sun, D.; Yu, Y. Automatic cloud-shadow removal from flood/standing water maps using MSG/SEVIRI imagery. *Int. J. Remote Sens.* **2013**, *34*, 5487–5502. [[CrossRef](#)]
29. Li, S.; Sun, D.; Goldberg, M.D.; Sjoberg, W. Object-based automatic terrain shadow removal from SNPP/VIIRS flood maps. *Int. J. Remote Sens.* **2015**, *36*, 5504–5522. [[CrossRef](#)]
30. Li, S.; Sun, D.; Goldberg, M.D.; Sjoberg, W.; Santek, D.; Hoffman, J.P.; DeWeese, M.; Restrepo, P.; Lindsey, S.; Holloway, E. Automatic near real-time flood detection using Suomi-NPP/VIIRS data. *Remote Sens. Environ.* **2017**, *204*, 672–689. [[CrossRef](#)]
31. Temimi, M.; Leconte, R.; Brissette, F.; Chaouch, N. Flood and soil wetness monitoring over the Mackenzie River Basin using AMSR-E 37 GHz brightness temperature. *J. Hydrol.* **2007**, *333*, 317–328. [[CrossRef](#)]
32. Zheng, W.; Liu, C.; Wang, Z.X.; Xin, Z.B. Flood and waterlogging monitoring over Huaihe River Basin by AMSR-E data analysis. *Chin. Geogr. Sci.* **2008**, *18*, 262–267. [[CrossRef](#)]
33. Sun, D.; Li, S.; Zheng, W.; Croitoru, A.; Stefanidis, A.; Goldberg, M.D. Mapping floods due to Hurricane Sandy using NPP VIIRS and ATMS data and geotagged Flickr imagery. *Int. J. Dig. Earth* **2015**, *6*. [[CrossRef](#)]
34. Zheng, W.; Sun, D.; Li, S. Mapping Coastal Floods Induced by Hurricane Storm Surge using ATMS Data. *Int. J. Remote Sens.* **2017**, *38*, 6846–6864. [[CrossRef](#)]
35. Bates, P.D.; Wilson, M.D.; Horritt, M.S.; Mason, D.C.; Holden, N.; Currie, A. Reach scale floodplain inundation dynamics observed using airborne synthetic aperture radar imagery: Data analysis and modelling. *J. Hydrol.* **2006**, *328*, 306–318. [[CrossRef](#)]
36. Goldberg, M.; Li, S.; Goodman, S.; Lindsey, D.; Sjoberg, B.; Sun, D. Contributions of Operational Satellites in Monitoring the Catastrophic Floodwaters Due to Hurricane Harvey. *Remote Sens.* **2018**, *10*, 1256. [[CrossRef](#)]
37. Goldberg, M.; Li, S.; Lindsey, D.; Sjoberg, B.; Zhou, L.; Sun, D. Mapping, Monitoring, and Prediction of Floods Due to Ice Jam and Snowmelt with Operational Weather Satellites. *Remote Sens.* **2020**, *12*, 1865. [[CrossRef](#)]
38. Guha-Sapir, D.; Rodriguez-Llanes, J.M.; Jakubicka, T. Using disaster footprints, population databases and GIS to overcome persistent problems for human impact assessment in flood events. *Nat. Hazards* **2011**, *58*, 845–852. [[CrossRef](#)]
39. Xian, G.; Homer, C.; Dewitz, J.; Fry, J.; Hossain, N.; Wickham, J. The change of impervious surface area between 2001 and 2006 in the conterminous United States. *Photogramm. Eng. Remote Sens.* **2011**, *77*, 758–762.
40. Tatem, A.J. WorldPop, open data for spatial demography. *Sci. Data* **2017**, *4*, 170004. [[CrossRef](#)] [[PubMed](#)]
41. Clark, M.J. Putting water in its place: A perspective on GIS in hydrology and water management. *Hydrol. Process.* **1998**, *12*, 823–834. [[CrossRef](#)]
42. Zerger, A.; Wealands, S. Beyond modelling: Linking models with GIS for flood risk management. *Nat. Hazards* **2004**, *33*, 191–208. [[CrossRef](#)]
43. Peduzzi, P.; Dao, H.; Herold, C.; Mouton, F. Assessing global exposure and vulnerability towards natural hazards: The disaster risk index. *Nat. Hazards Earth Syst. Sci.* **2009**, *9*, 1149–1159. [[CrossRef](#)]
44. The VIIRS Flood Products at the SSEC's Real Earth. Available online: <https://www.ssec.wisc.edu/flood-map-demo/flood-products/> (accessed on 24 August 2020).
45. JPSS Proving Ground Global Flood Products Archive. Available online: <https://jpssflood.gmu.edu/> (accessed on 24 August 2020).

